A scenario for torus T^2 destruction via a global bifurcation

T. Pereira [a,b], M.S. Baptista [b,*], M.B. Reyes [a], I.L. Caldas [a],
J.C. Sartorelli [a], J. Kurths [b]

[a] *Instituto de Física, Universidade de São Paulo, Caixa Postal 66318, 05315-970 São Paulo, SP, Brazil*
[b] *Nonlinear Dynamics, Institute of Physics, University of Potsdam, D-14415, Potsdam, Germany*

Accepted 22 June 2007

Abstract

We show a scenario of a two-frequency torus breakdown, in which a global bifurcation occurs due to the collision of a quasi-periodic torus T^2 with saddle points, creating a heteroclinic saddle connection. We analyze the geometry of this torus-saddle collision by showing the local dynamics and the invariant manifolds (global dynamics) of the saddle points. Moreover, we present detailed evidences of a heteroclinic saddle-focus orbit responsible for the type-II intermittency induced by this global bifurcation. We also characterize this transition to chaos by measuring the Lyapunov exponents and the scaling laws.
© 2007 Elsevier Ltd. All rights reserved.

1. Introduction

Non-linear phenomena are abundant in nature. It has been extensively studied in several areas of physical sciences [1], economy [2], ecology [3] and applied engineering [4]. The behavior of a non-linear oscillator may change as we vary a control parameter; the oscillator undergoes a bifurcation, causing a change in the topological picture of the solution in the phase space, thus altering the dynamics. Bifurcations can be local (changing only locally the behavior of the oscillator in the phase space) or global (changing the behavior of phase space as a whole). The understanding of the bifurcation scenario for an oscillator is particularly important for the characterization of its dynamical behavior. Surprisingly, there are just a few bifurcation scenarios in which a non-linear oscillators initially presenting a periodic behavior can undergo a transition to chaos. These transitions has been studied in conservative [5] and dissipative systems [6,1].

Among the routes to the appearance of chaotic behavior are the bifurcations of a quasi-periodic attractor with N incommensurate frequencies, also known as torus T^N. Landau proposed the motion on such high-dimensional torus as the basic mechanism to create turbulence; as a parameter is increased towards the turbulence, successive modes of incommensurate frequencies would arise. In this situation, the dynamics of this higher-dimensional torus would be regarded as a model for turbulence. But, Newhouse–Ruelle–Takens [8] showed that turbulence can already arise from the destabilization of a low-dimensional three-frequencies torus T^3. They showed that small perturbations on

---

* Corresponding author.
E-mail address: murilo@mpipks-dresden.mpg.de (M.S. Baptista).

the constant vector field of the T^3 are enough to create chaos by torus destruction, resulting in a dynamics that presents infinitely many frequencies. This bifurcation explains the appearance of chaos from a torus of three or more frequencies but does not hold for a low-dimensional torus T^2. So, one could expect that chaos does not appear by the destabilization of a T^2 torus, but this is not the case.

Curry and Yorke [9] showed that chaos, with broadband spectra, could emerge directly from the destabilization of a torus T^2. This scenario is characterized by a T^2 born from the destabilization of a stationary solution, followed by a successive series of phase-lockings and, eventually, the onset of chaos. The emergence of chaotic behavior is generally associated to the appearance of a localized folded and wrinkled structure, as reported in laser systems [10] and in line-coupled diodes [11]. A frequency characterization of this type of chaos shows that the frequencies present before the torus breaks are still dominant in the chaotic trajectory. A metric characterization shows the appearance of an extremely small and positive Lyapunov exponent.

Recently, it was shown the appearance of chaotic behavior by a transition directly from the torus T^2 [12–14], in which there is a collision of the torus with saddle points originating a type-II intermittency [15]. In this scenario, there is a mechanism of reinjection associated to a heteroclinic connection between the central unstable focus and the saddles, which takes the trajectory back to the vicinity of the focus. This trajectory evolves in a laminar fashion around the focus towards the saddles. It behaves chaotically in the saddles vicinity, and far away from the region delimited by these saddles, returning to the focus along the heteroclinic orbit. This alternation between this type of laminar and chaotic behavior characterizes the type-II intermittency.

The breakdown of the torus T^2 by a torus-saddle collision differs from the Curry–Yorke in the sense that it is associated with the appearance of many frequencies, where the old frequencies no longer play an important role. Additionally, a global bifurcation creates a robust heteroclinic cycle with the appearance of a very large positive Lyapunov exponent. As reported by Lethelier et al. [16], this phenomenon is not restricted to continuous-time systems but it also happens in spatiotemporal systems.

In this work, we review this scenario of T^2 breakdown [12–14] and, in addition, we present details of the methods previously used to characterize such a scenario. We especially analyze the global dynamics: the collision of the torus with the saddle forming a heteroclinic saddle connection, the non-linear mechanism responsible for the type-II intermittence. We also characterize the local dynamics: the existence of the focus and saddle points, i.e. the stretching and the folding character of the saddle vicinity and the spiraling character of the focus vicinity. As the parameter is varied and the torus T^2 grows in size, the positions of the saddle points remain almost unaltered. So, it is the torus that approaches the saddle points and not vice-versa.

This work is organized as follows. In Section 2 we present the forced Chua's circuit and in Section 3 the experimental set-up. In Section 4 we show the experimental results that support the numerical scenario shown in Section 5. The conclusions are given in Section 6.

2. Forced Chua's circuit

The forced Chua's circuit constructed and analyzed in this work was introduced in [17,12]. The circuit and the characteristic curve of the piecewise-linear resistor R_{NL} are schematically shown in Fig. 1. This circuit is well known [20] and it is basically a RLC oscillator (a) with a non-linear active component, the R_{NL} (b).

This circuit is composed of two capacitors, C_1 and C_2, two resistors, R and r, one inductor, L, and the non-linear (piecewise-linear) resistor, R_{NL}. V_{c1}, V_{c2}, and i_L represent the tension across the capacitors, and the current through the inductor, respectively. The R_{NL} characteristic curve is mathematically represented by:

$$i_{NL}(V_{c1}) = m_0 V_{c1} + 0.5(m_1 - m_0)\{|V_{c1} + B_p| + |V_{c1} - B_p|\}. \tag{1}$$

The forcing applied to the circuit, shown in Fig. 1 is of the form $V \sin(2\pi f\, t)$, where V is the amplitude and f is the frequency.

3. Experimental setup

The non-linear resistor is constructed such that the characteristic curve presents $m_0 = -0.539(3)$, $m_1 = -0.910(2)$, and $B_p = 1.200(4)$ V (the number between brackets indicate the deviation in the last digit). The components of the circuit are $C_1 = 0.0047\ \mu F$, $C_2 = 0.052\ \mu F$, $R \in [1.0, 1.7]\ K\Omega$, $L = 9.2$ mH, and $r = 10\ \Omega$. We set the resistor R to obtain the regime of a Double-Scroll-like attractor, and then we introduce the perturbation destroying this attractor, which gives place to the attractors observed in this work.
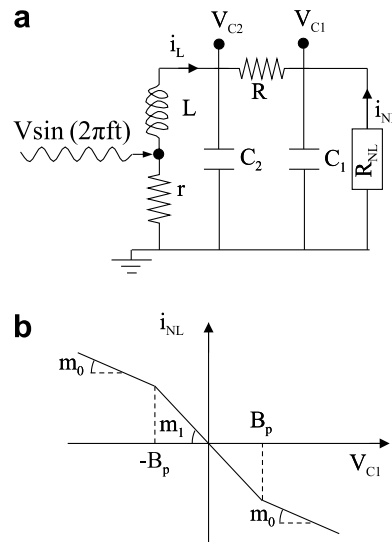
Fig. 1. (a) Forced Chua's circuit, the forcing is represented by $V_p \sin(2\pi f_p t)$ and (b) the piecewise-linear characteristic curve of the resistor R_{NL}.

We use a Tektronix AFG320 function generator connected in parallel to the resistor r, to introduce the forcing in the circuit. An Agilent 35670 A dynamic signal analyzer is used to check the frequency f of the circuit, by a Fourier transformer in the variable V_{c1}. Data acquisition is performed using an AT-MIO 16E1 National Instruments board (12 bits) connected to a computer controlled by a software developed in LabView language, for a sampling of $\delta = 1/250$ kHz.

We acquire the variable $V_{c_1}(t = i\delta)$, with i representing the number of acquired data points. Next, we identify all its local maxima, which is the variable chosen to reconstruct the attractor.

These maxima are obtained by fitting a 2 degree polynomial to a set of 15 points of the experimental time series. Then, it is verified whether the maximum of the fitting curve is within the time interval corresponding to the used time series. If so, this maximum point of the fitting is taken as a local maximum $V_{c_1}(n)$ where the n index represents the number of maxima. This time series $V_{c1}(n)$ is used to reconstruct the attractor $V_{c_1}(n) \times V_{c_1}(n+p)$, using time-delay embedding coordinates [18]. The parameter p represents the time-delay for the embedding space. The value p is chosen conveniently according to the geometry of the attractor studied, here $p = 2$. This reconstruction is a two-dimensional map of the attractor. Thus, the torus T^2 appears as a cycle in this representation and a limit cycle as a point.

4. Experimental torus-saddle collision

We use as control parameters the voltage V and frequency f of the forcing. The behavior of the forced circuit is very rich and complex. In the parameter space several windows of phase-locking emerge when we change these parameters [19]. In particular at $V = 0.7$ V and $f = 3500$ Hz, a periodic window is obtained and we explore this situation in details. For $V = 0.7$ V fixed, we change f within the interval $[3505, 3537]$ Hz and built the bifurcation diagram as shown in Fig. 2. The periodic window remains up to $f = 3514$ Hz, when a Hopf bifurcation occurs, so a torus T^2 takes place. Further increasing the control parameter, at $f = 3530.6$ Hz a sudden change in the system dynamics happens, the destruction of the torus by a torus-saddle collision.

In Fig. 3a, we show a torus T^2 created from a Hopf bifurcation of a limit cycle. In the used two-dimensional reconstruction this bifurcation corresponds to an attracting fixed point becoming an unstable focus. Close to the Hopf bifurcation point, the torus has a circular shape with the average radius, $\langle r \rangle$, that scales as $\langle r \rangle \propto (f - f_c)^{\frac{1}{2}}$ as f is increased, with f_c being the parameter for which the bifurcation occurs. As the parameter is increased further, the torus shape becomes like a pentagon, Fig. 3b. This change happens when the torus grows and gets close to the five fixed points corresponding to a period-5 unstable saddle orbit.

At a critical parameter $f = 3530.6$ Hz, the torus collides with the external saddle points. Fig. 3c shows a parameter situation in which the torus has already collided with the saddles. In this figure, the diamonds outside of the broken torus represent the scaping of the trajectory from the broken torus, along the unstable manifolds of the saddle points.
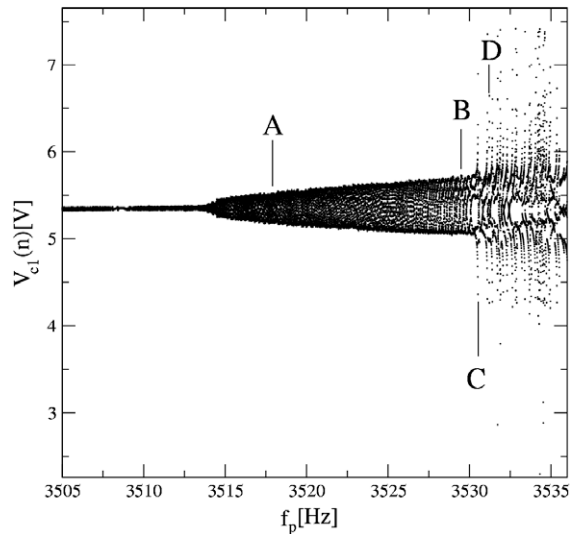
Fig. 2. Bifurcation diagram of the forced Chua's circuit, for $V = 0.7$ V. One sees a fixed point that bifurcates by a Hopf bifurcation into a torus T^2. At a critical parameter $f = 3530.6$ Hz (indicated by the letter C) a torus-saddle collision happens. The attractors indicated by the letters (A–D) are shown in Fig. 3.

Analyzing the destroyed torus, depicted in Fig. 3d, we can see that the dynamics is still related to the torus. In fact, the trajectories behave as if they were in a quasi-periodic oscillation, around the saddle points, for a while. Thus, they go away from the saddle vicinity along the saddle unstable manifolds, spending some time far away from the region delimited by the saddles. Then, they are eventually reinjected in the unstable focus vicinity, spiraling toward the saddle points. Then, this cycle repeats itself. This process is the characteristic mechanism of type-II intermittency.

This unstable focus is obtained by the Fixed Point Transform [21], which consists in transforming the original data set, such that the transformed data is concentrated on the periodic orbits. The histograms of the transformed data presents sharp peaks at the location of the unstable periodic orbits, which allow us to estimate their positions.

The focus point is represented in Fig. 3c by a diamond inside the broken torus. The existence of the saddle points, near this distorted torus, can be verified by introducing a small noise in the forced Chua's circuit. This is done by approaching a magnet in the inductor. This causes a change in the magnetic flow of the inductor, which induces a small change in a dynamical variable, taking the trajectories away from the attractor. With this procedure we are be able to place the trajectory in the vicinity of the saddle points, as well as, everywhere else in the phase space. We repeat this perturbation until we have a picture of the phase space in which we can clearly see the saddle points. Those are identified by selecting trajectory points that after p-iterations are mapped close by. In Fig. 4 we show the torus and the perturbed trajectories that are placed in the vicinity of the saddles. After reaching the saddle vicinities, the trajectory goes either toward the torus or away from it, by the unstable manifolds of the saddle points, following the directions indicated in this figure by the arrows.

The approach of the T^2 to the saddle points causes a change in the dynamics that can be observed by the time the system spends in each part of the torus. The more distorted the attractor becomes, the more time the trajectory remains close to each torus corner. From the time series of maxima $V_{c_1}(n)$, we construct a k-return map $\theta_n \times \theta_{n+k}$, where θ is the angle between the trajectory and the inner unstable focus, and k is chosen in accordance to the rotation number. A representation of this angular variable is shown in Fig. 3b, which is used to show the permanence of the trajectory in the vicinity of the saddle points, which can be seen in the return map of Fig. 5. This return map reveals five regions which are mapped close to the identity line. The trajectory takes more time to leave the vicinity of these tangent points than in any other place. The local geometry of the mapping around the saddle points can be analyzed by observing the return of a set of initial conditions, around these saddles, after five iterations. In Fig. 6, we connect the points in the set of initial conditions to the corresponding returning points. We have selected the shortest arrows in order to not overwhelming the picture. This technique completely reveals the dynamical structure around the saddle points.

Now, we argue that the trajectories in the branches of the broken torus, the extended structures in Fig. 3d, are ruled by the unstable manifold of the saddle points. To see this, we evolve in time a set of points in the branch, close to the saddle, and after for example 15 iterations this small ball returns to the branch, but stretched. So the trajectories in the
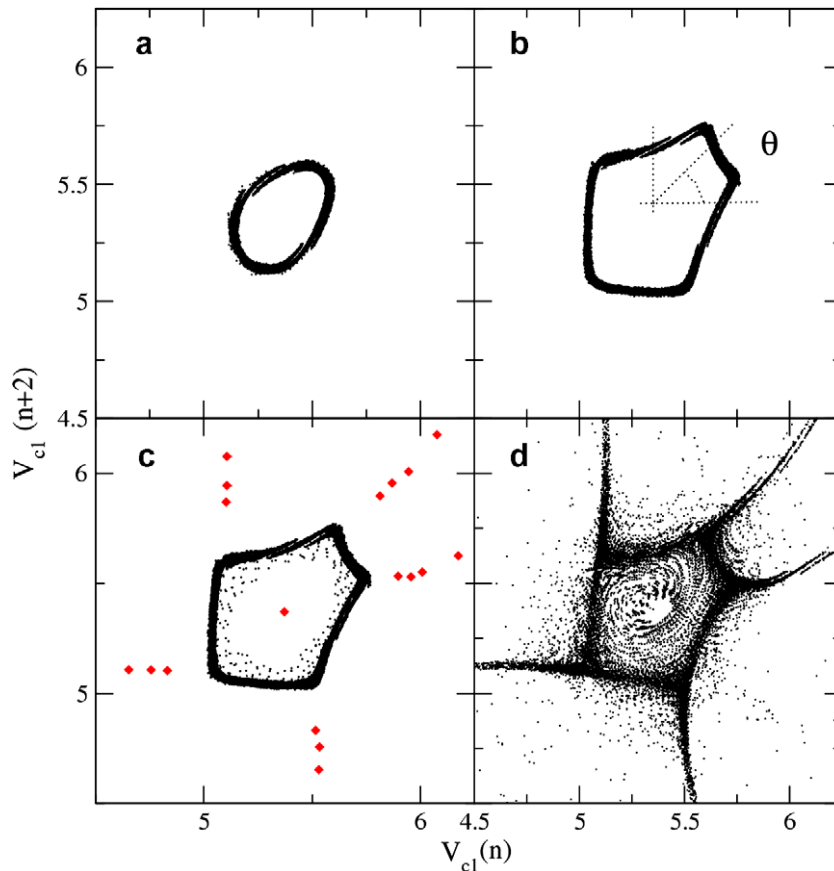
Fig. 3. (a) A torus T^2 is shown, for $f = 3518$ Hz. In (b) the torus becomes like a pentagon, due to the manifolds of the unstable saddle points, near the torus, for $f = 3529$ Hz. In (c) we show the attractor right after the torus has collided with the saddle points. The diamond points are a first scape of an orbit from the broken torus, and the central point inside the torus is a repeller focus, obtained by a Point Fixed Transformer, for $f = 3530$ Hz. In (d), the chaotic attractor born from a global bifurcation, the torus-saddle collision, for $f = 3531$ Hz.

branches are governed by an unstable manifold. Following the consecutive iterates of the branches, we notice that the points on the branches are eventually mapped on the vicinity of the focus.

A schematic view of the dynamics of trajectories in the broken torus is shown in Fig. 7. We illustrate the manifolds of the saddles points, and some orbits leaving the unstable focus, toward the saddle points. The placement of the trajectory around the focus happens associated with a heteroclinic orbit connecting the saddle points with the central unstable focus. So, the unstable manifold of the saddle are eventually mapped in the focus.

The scaping of the trajectory from the saddles (chaotic bursts) and the subsequent reinjections around the focus can be also recognized in the time series $V_{c1}(n)$, in Fig. 8, where one can see that the orbits spiral out from the center, getting closer to the saddle points, followed by a chaotic burst. Eventually, they are reinjected around the focus along the heteroclinic orbit, generating the characteristic behavior of the type-II intermittency.

As idealized by Pomeu and Manneville [15], the type-II intermittence is born with a Hopf bifurcation in such a way that the steady state goes to an oscillatory behavior, the trajectory spiraling around the focus, followed by chaotic bursts. To generate intermittence they conjectured a non-linear mechanism of reinjection. However, in some situations [22,12,13], it can happen that after the Hopf bifurcation the oscillatory behavior is still stable, and only after some variation in the control parameter the intermittent behavior takes place, which is the case of our experiment.

When the torus looses its stability and the intermittent behavior takes place, one can still write the same normal form as for the inverse pitchfork bifurcation [5], since one has an analogous resonance condition on the eigenvalues of the unstable focus. So, in the presence of a global mechanism which set the trajectory in the vicinity of the focus, the usual analysis of the laminar time statistics can be applied.
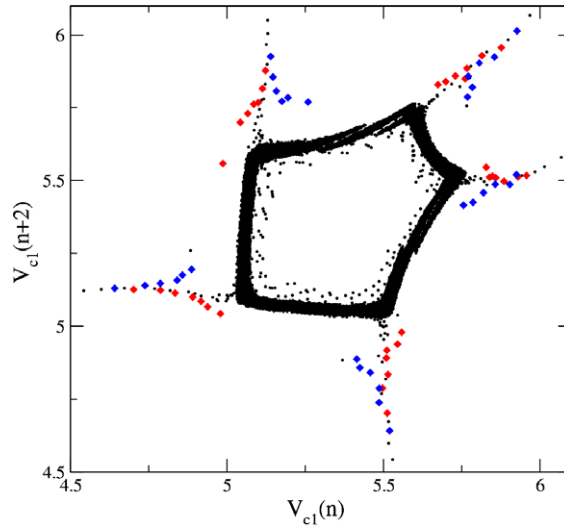
Fig. 4. At $f = 3529$ we introduce a small noise in the magnetic flow of the inductor. This take the trajectories away from the torus and reveals the structure of the phase space near the torus, i.e., the existence of the saddles.
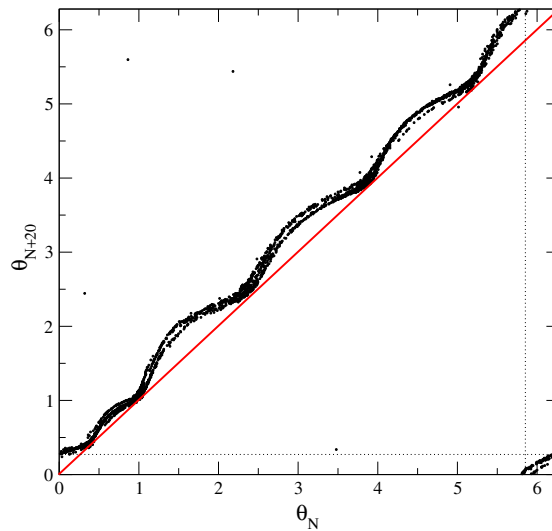

Fig. 5. Return map of the 20th iterate. This enable to detect five points which are mapped very close to themselves, and the system spends more time at these points. These points are related to the corners of the pentagon-shape attractor in Fig. 3d, showing that the attractor settles close to an unstable period-5 saddle orbit.

The scaling law expected in the type-II intermittence is not fixed, in other words, given the average laminar time τ and $\epsilon = |f - f_c|$, the scaling $\tau \propto \epsilon^\mu$ depends on the approximation done in order to get the scaling law. As shown in Ref. [5], the exponent can vary from $\mu = -1/2$ to $\mu = -1$.

The average laminar time τ may be difficult to be estimated since the determination of the laminar period can be mislead by the fact that we are working in a projection of the full phase space. Therefore, we rather compute a more robust quantity called γ [22]. Thus, instead of measuring the laminar time we measure the chaotic bursts, γ is the fraction of the time of the chaotic burst $\gamma = t_{\text{burst}}/t_{\text{total}}$ and, as the chaotic burst is very pronounced, the statistics of is better. Assuming $\tau \propto \epsilon^{-\mu}$, the variable γ is related to τ by
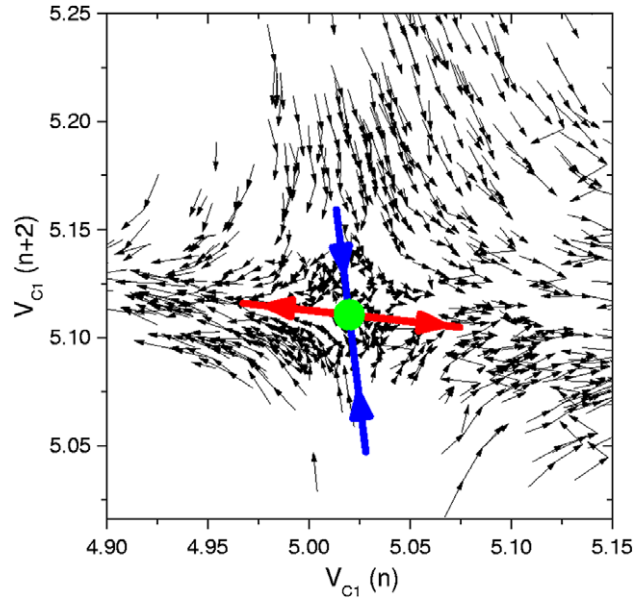
Fig. 6. The arrows connect a given point with its 5th iterate. One can see the saddle structure represented by the arrows, the unstable (stable) manifold is revealed by looking at the direction of the vectors. The filled circle indicates the saddle point position and the oversized arrows indicate the unstable and stable manifolds of the saddle point.
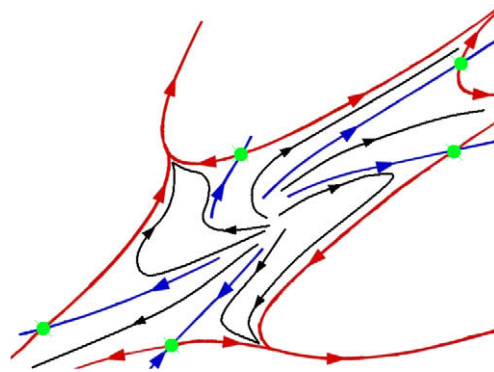

Fig. 7. We illustrate the dynamics of the 5th iterate of the broken torus. We show the manifolds of the saddle points, and some orbits that departure from the focus and go toward the saddle points.

$$\gamma = \left(1 + \frac{d}{\epsilon^{\mu}}\right)^{-1} \tag{2}$$

with d being a constant (see Ref. [22] for more details). Since $1 \ll d/\epsilon^{\mu}$, Eq. (2) can be written as $\gamma \propto \epsilon^{\mu}$. From our experimental results we have that $\mu \approx 0.97$ (Fig. 9), which suggests that the observed scenario is of a type-II intermittence.

Next, we estimate the Lyapunov exponents of our data through the Eckmann–Ruelle technique [7], using the well known definition of the Lyapunov exponents:

$$\lambda_j = \lim_{N \to \infty} \frac{1}{N} \ln |\Lambda_j^N|, \tag{3}$$

where Λ_j^N are the eigenvalues of the matrix $\mathbf{M}$ and

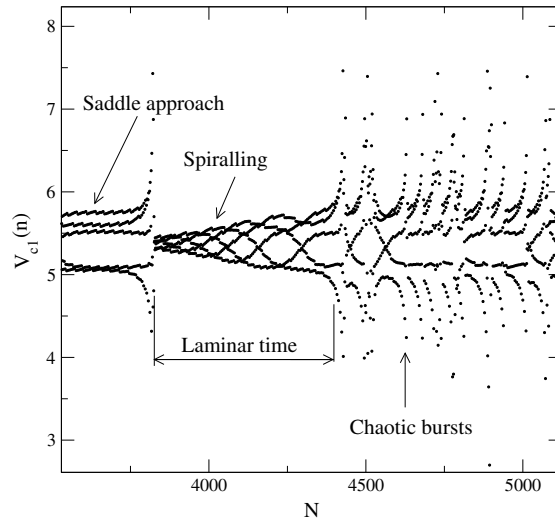$$\mathbf{M} = \prod_{n=1}^{N} \mathbf{J}(\mathbf{x}_n), \tag{4}$$

Fig. 8. Time series of the maxima for $V_p = 0.7$ and $f_p = 3531$. After the trajectory escapes from the saddle neighborhood along the unstable manifold, it behaves chaotically (chaotic bursts) until its reinjection around the unstable focus. Thus, it spirals toward the saddles in a laminar fashion.
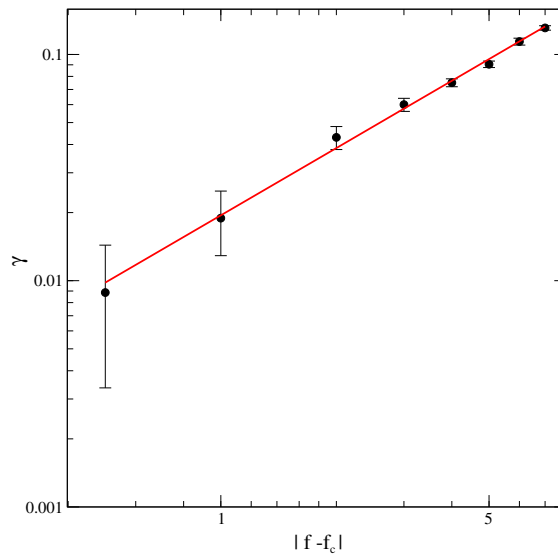

Fig. 9. We show $\log \gamma \times \log|f - f_c|$. By fitting the data set, we have that the average laminar time scales as $\tau \propto |f - f_c|^\mu$, where $\mu \approx 0.97$, which agrees with the interpretation of type-II intermittence.

where x_n represents a vector with coordinates $\{V_{c1}(n), V_{c1}(n + 2)\}$, and $\mathbf{J}(\mathbf{x}_n)$ is a linear transformation that places the points in the vicinity of $\mathbf{x}_n$ to the $\mathbf{x}_{n+1}$. If the Jacobian is invertible we can write it in the form:

$$\mathbf{J} = \mathbf{OT}, \tag{5}$$

where $\mathbf{O}$ is an orthogonal matrix and $\mathbf{T}$ is a triangular matrix (if an specific matrix is not invertible, we eliminate it from the calculus). We can do a partition by the QR decomposition technique. So, we are able to write:

$$\mathbf{J}_n = \mathbf{O}_n \mathbf{T}_n \mathbf{O}_{n-1}. \tag{6}$$

Therefore, $\mathbf{M}$ can takes the form:

$$\mathbf{M} = \mathbf{O}(x_n)\mathbf{T}(x_n)\mathbf{T}(x_{n-1})\dots\mathbf{T}(x_1). \tag{7}$$

Now, the Lyapunov exponents can be written as

$$\lambda_j = \frac{1}{N} \sum_{n=1}^{N} \ln |T_{jj}(\mathbf{x}_n)|. \tag{8}$$

The spectra of the Lyapunov exponents, for the forced Chua's circuit has the form $\Lambda = (\lambda_1, 0, \lambda_2, -c)$. The null exponent corresponds to the direction of the flow, and the $-c$ exponent corresponds to the strong stable foliation. The other two exponents, λ_1 and λ_2, correspond to the stretching and the folding dynamics of the return map $V_{c1}(n) \times V_{c1}(n+2)$. The spectrum that corresponds to the attractor of Fig. 3d is $\lambda_1 = 0.30 \pm 0.08$ and $\lambda_2 = -0.1 \pm 0.04$, with one positive Lyapunov exponent, and therefore chaotic behavior.

5. Numerical results

In order to have a better understanding of the system we perform numerical analysis of the circuit equations, with parameters that adequately reproduce the experimental scenario. The equations that describe the system shown in Fig. 1 can be obtained by applying the Kirchoff's laws to the nodes of the circuit. These equations are not autonomous, due to the time dependence of the perturbation. However, adding one more equation we put the system of differential equations in an autonomous form. The resulting state equations are given by

$$C_1 \frac{dV_{c1}}{dt} = \frac{1}{R}(V_{c2} - V_{c1}) - i_{NR}(V_{C1}), \tag{9}$$

$$C_2 \frac{dV_{c2}}{dt} = \frac{1}{R}(V_{c1} - V_{c2}) + i_L, \tag{10}$$

$$L \frac{di_L}{dt} = -V_{c2} - V \sin \phi, \tag{11}$$

$$\frac{d\phi}{dt} = f, \tag{12}$$

where V_{c1} and V_{c2} are the voltage in the capacitors C_1 and C_2, respectively, and i_L is the electric current across the inductor L. The analysis is done at the Poincaré section $V_{c1} = -1.5$. For each n crossing of the trajectory we have a pair of points $\{V_{c2}(n), i_L(n)\}$.
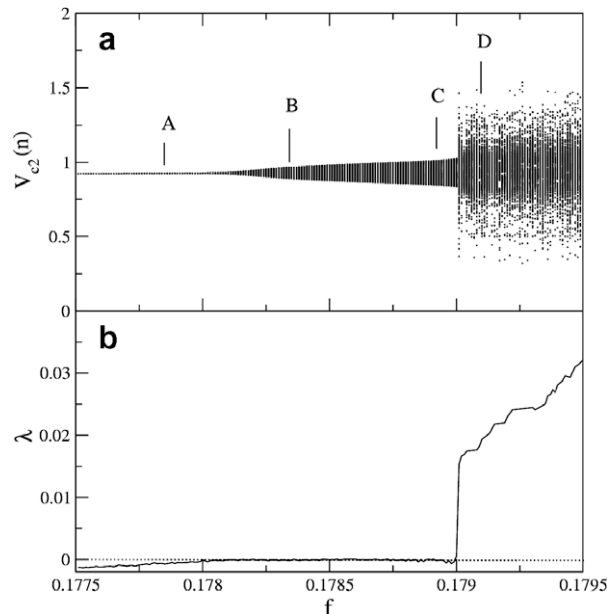

Fig. 10. (a) Numerical bifurcation diagram, similar to the one experimentally observed, Fig. 2. The letters (A–D) indicate the attractors which are depicted in Fig. 11. (b) Largest Lyapunov exponent. At a critical parameter, $f \approx 0.179$, one can see an abrupt transition of the largest Lyapunov exponent.

For convenience, we introduce the usual parameter rescaling which produces a set of dimensionless parameters [19]. We permit a slight modification of the rescaled parameters due to deviations in the real experimental values. Thus, the parameters used in the numerical simulation of the circuit of Fig. 1 are $C_1 = 0.1$, $C_2 = 1.0$, $L = 1/6$, $\frac{1}{R} = 0.575$, $m_0 = -0.5$, $m_1 = -0.8$, and $B_p = 1.0$. We integrate the forced Chua's equations by using the 4th order Runge-Kutta method with an integration step of 0.01.

5.1. Unstable periodic orbits

In order to detect the saddle points as well as the focus, we introduce a numerical technique, which can be adapted to experimental data series. The method consists in integrating the equations for several trials and changing the initial condition in each trial. The initial conditions are randomly chosen within a volume centered at a point p_0 in the chosen Poincaré section of the phase space. The point p_0 has to be close to the searched period-n unstable orbit.

Each integration trial is performed until the trajectory, departing from these initial conditions, returns to the Poincaré section after the next nth crossings. The distance between the initial condition and the returning point is measured and compared with the previous trials. The point p_0 is thus replaced by the initial condition that has the minimal absolute distance with the returning trajectories. The initial conditions are now randomly chosen around this new center p_1. We repeat this process i times until the distance between the initial condition and a returning point is smaller than 10^{-8}.

If the system performs $i = 5000$ trials without changing the point p_i, the range in which the initial conditions are chosen is decreased by a factor of β, here $\beta = 0.8$, meaning that the overall volume is decreased by a factor of β^d, where d is the dimension of the phase space. This is required because the bigger is the volume of search the smaller is the probability
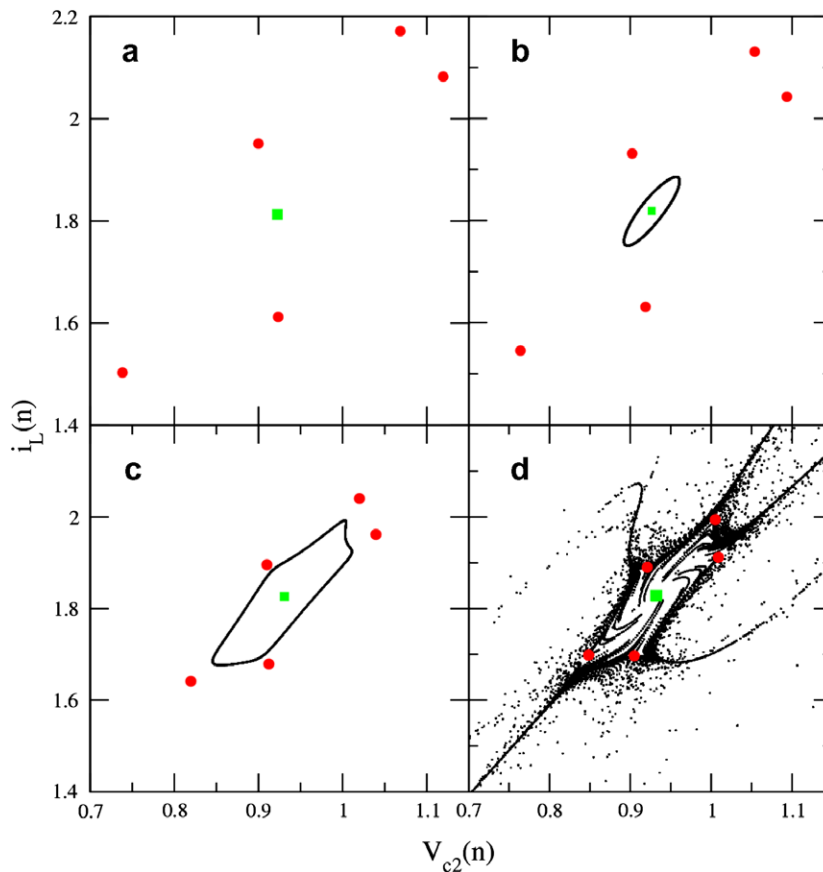

Fig. 11. Simulation of the experimental attractors observed in Fig. 3. The saddle points are indicated by filled circles and the focus by a filled square. In (a) it is shown a fixed point, for $f = 0.17785$. In (b) the torus is born from a Hopf bifurcation, for $f = 0.17832$. In (c) one can see the deformation in the torus due the presence of the saddle points, for $f = 0.17893$. In (d) it is shown the destroyed torus, for $f = 0.1791$. The attractors in this figure are obtained for a fixed $V = 0.234$.

of finding a better central point p_i. Since during the trials both the initial conditions and their respective returning points are saved, it is possible to figure out how the space is mapped near the fixed points.

This method is not convergent for all points, since the center of search p_i can be mistaken by a recurrent orbit, that is not periodic. That can be avoided with a previous analysis of the system, and a suitable estimation of the initial central point and volume, around a region where an unstable periodic orbit seems to exist.

This method is applied throughout this section to obtain the unstable periodic orbits and their fixed points, i.e., their intersections with the Poincaré section presented later on.

5.2. Numerical picture

We fix the perturbation amplitude at $V = 0.234$, and change the frequency in the interval $f = [0.1775, 0.1795]$. We analyze the system dynamics in a Poincaré section at $V_{c_1} = -1.5$, and in Fig. 10 a we show the bifurcation diagram plotting $V_{c_2}(n)$ versus f, and in Fig. 10b we show the maximum Lyapunov exponent as a function of the control parameter f.
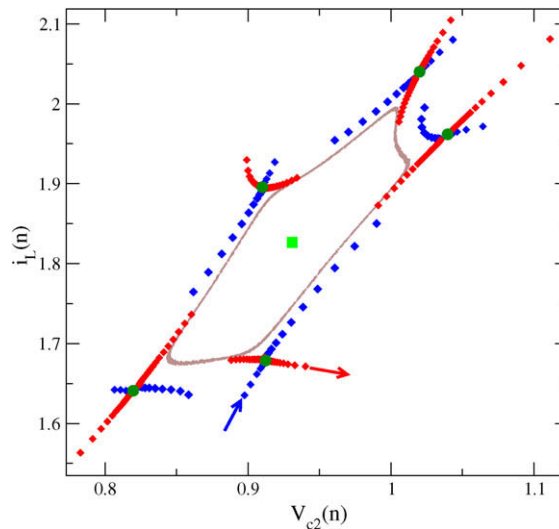

Fig. 12. We show the same torus shown in Fig. 11c with the unstable focus (light gray square), the saddle points (gray circles), and a picture of the manifolds of the saddle points the stable direction (squares) and the unstable direction (triangles). The manifolds are depicted by iterating a set of initial conditions very close to one saddle point.
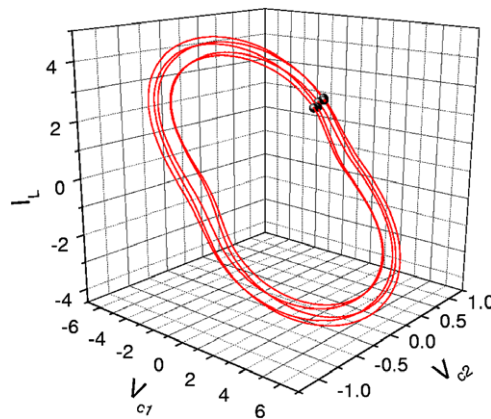

Fig. 13. The unstable periodic orbit of the chaotic flow responsible for the saddle points in Fig. 11d.
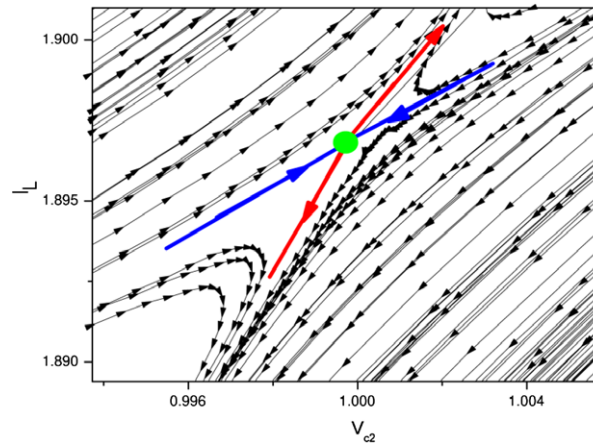
Fig. 14. Local structure around the 5-period orbit saddle orbit. We connect a given point near the saddle and its 5th iterate by an arrow.

In Fig. 11 the Poincaré section of the attractors indicated by letters (A–D) in Fig. 10 is given. We also show the saddle points, depicted by the filled circles (gray), and the focus depicted by a filled square (light gray). These periodic points are obtained by the method proposed previously. In Fig. 11b, after a Hopf bifurcation that happens at $f = 0.1781$, a torus T^2 takes place. This Hopf bifurcation is a local bifurcation, so it does not change the structure of the phase space far away from the bifurcation point.

As the torus approaches the saddle points, it becomes distorted due to the presence of these points, Fig. 11c. We manage to get an illustration of the manifolds of the saddle points. For that, we evolve forward and backward a small set of initial condition, very close to a saddle point. The result is shown in Fig. 12, where we depict the torus showed in Fig. 11c and the trajectories of these initial conditions chosen near the saddle. The unstable periodic orbit containing the 5 saddle points of Fig. 12 is presented in Fig. 13 together with saddles indicated by the filled circles. The local dynamics around the saddle points can be seen in Fig. 14. In this figure, by the tick arrows represent the local linear geometry around the saddle, i.e., the stable (dark gray) and unstable eigenvectors (gray) of the saddle. The local geometry is depicted likewise done in Fig. 6. We iterate a set of initial conditions around the saddle and connect the returning points to the Poincaré section with arrows that are not too large ($<10^{-3}$) in length. This procedure reveals the local structure around the saddle, indicating the stretching and expanding character of the saddle point.

We also numerically obtain a scaling law for the average laminar length $\langle T \rangle$ of the type-II intermittency observed in the attractor depicted in Fig. 11d, for $V = 0.234$. Analogously to the experimental scaling, we obtain $\langle T \rangle \propto |f - f_c|^{-\gamma}$, with $\gamma = 0.98 \pm 0.08$. Note the agreement between the experimental and numerical exponents. We also calculate the Lyapunov exponent of the attractor depicted in Fig. 11d, obtaining $\lambda_1 = 0.37 \pm 0.06$ and $\lambda_2 = -0.35 \pm 0.05$.

6. Conclusions

In this article we have analyzed experimentally and numerically the scenario of a two-frequency torus breakdown by a global bifurcation, the saddle-torus collision, in the forced Chua's circuit. This scenario is characterized by the collision of a quasi-periodic torus with saddle points. The torus is surrounded by the saddle points. As a parameter is increased, the torus grows in size and touches the saddle points. At the collision, the trajectory spends some time at the previous neighborhood of the torus, being spelled off the torus region by the unstable manifolds of the saddle points, the chaotic explosion, eventually returning to the neighborhood of the focus. At the moment of the collision a heteroclinic orbit is formed between the saddle and the inner unstable focus, it is responsible for the reinjection of the trajectory from the saddle to the focus. Then, the trajectory spirals off toward the saddle, the laminar phase, being again expelled, from the saddle manifolds. This endless repeating process between the laminar phase and chaotic explosion characterizes the type-II intermittency, phenomena borne together with this bifurcation.

We present experimental and numerical new details of this scenario, previously observed in [12–14]. These are mainly: (i) the existence of the saddle points. They are experimentally observed by introducing a perturbation in the circuit, at a moment that the saddle points are close to the T^2 torus. They are numerically detected by the method introduced in here:

(ii) The existence of the focus points. They are experimentally obtained by the method of Ref. [21], and numerically by the method introduced in here; (iii) The manifolds of the saddle points. We also show evidences of the heteroclinic orbit between the saddle points and the focus, by iterating points at the unstable manifold of the saddle and verifying that they eventually are mapped in around the focus; (iv) We obtain the Fourier and the Lyapunov spectra, showing that both suffer a sudden transition at the moment of the torus collision; (v) Verification of a power scaling law for the average laminar length, $\langle T \rangle$ with respect to the distance between the parameter, f (perturbing frequency), and the critical parameter, f_c, where the bifurcation takes place. We find that $\langle T \rangle \propto |f - f_c|^{-\mu}$, with $\mu = 0.97 \pm 0.05$ (experimentally) and $\mu = 0.98 \pm 0.08$ (numerically).

Acknowledgements

References

[1] Ott E. Chaos in dynamical systems. Cambridge: Cambridge University Press; 1993;
    Alligood KT, Sauer TD, Yorke JA. Chaos, an introduction to dynamical systems. New York: Springer; 1997.
[2] De Grauwe P, Wachter H, Embrechts M. Exchange rate theory: chaotic models of foreign exchange markets. Oxford: Blackwell; 1993.
[3] Blasius B, Stone L. Nature 2000;406:846;
    Blasius B, Stone L. Nature 1999;399:354.
[4] Costelloa BL, Adamatzkyb A. Chaos, Solitons & Fractals 2005;25:535;
    Meisner MJ, Frantziskonis GN. Chaos, Solitons & Fractals 1997;8:151.
[5] Lichtenberg AJ, A Lieberman M. Regular and stochastic motion. New York: Springer-Verlag; 1983. chapter 4.
[6] Eckmann J-P. Rev Mod Phys 1981;53:643.
[7] Eckmann J-P, Ruelle D. Rev Mod Phys 1985;57:617.
[8] NewHouse S, Ruelle D, Takens F. Comm Math Phys 1971;64:35.
[9] Curry JH, Yorke JA. Lect Notes Math 1978;688:48.
[10] Arecchi FT, Giacomelli G, Lapucci A, Meucci R. Phys Rev A 1991;43:4997.
[11] Yu Z, Steinshnier J, Littler CL, Perez M, Kowalski JM. Phys Rev E 1994;49:220.
[12] Baptista MS, Caldas IL. Phys Rev E 1998;58:4413.
[13] Baptista MS, Caldas IL. Physica D 1998;132:325.
[14] Pereira T, Baptista MS, Reyes MB, Caldas IL, Sartorelli JC, Kurths J. Phys Rev E 2006;73:017201.
[15] Pomeau Y, Manneville P. Comm Math Phys 1981;74:189.
[16] Lethelie C, Dinklage A, El-Naggar H, Wilke C, Bonhomme G. Phys Rev E 2001;63:042702.
[17] Itoh M, Murakami H, Chua LO. Int J Bifurc Chaos Appl Sci Eng 1994;4:1721.
[18] Takens F. In: Rand DA, Yang LS, editors. Lectures notes in mathematics, vol. 898. Berlin: Springer; 1981. p. 366.
[19] Baptista MS. PhD thesis, Universidade de São Paulo, Brasil; 1996.
[20] Madan RN. Chua's circuit: a paradigm of chaos. Singapore, River Edge, NJ: World Scientific; 1993.
[21] So P, Ott E, Schiff SJ, Kaplan DT, Sauer T, Grebogi C. Phys Rev Lett 1996;25:4705.
[22] Frank M, Schmidt M. Phys Rev E 1997;56:2423.